Se-Substitution and Cation Effects on the High-Pressure Molecular Superconducior, β-Me$_4$N[Pd(dmit)$_2$]$_2$ -A Unique Two-Band System

Reizo Kato [a] , You-Liang Liu [a] , Yuko Hosokoshi [a c] , Shuji Aonuma [a] & Hiroshi Sawa [b]

[a] The Institute for Solid State Physics, The University of Tokyo, Roppongi 7-22-1, Minato-ku, Tokyo, 106, Japan

[b] Department of physics, Faculty of Science, Chiba University, Yayoi-cho 1-33, Inage-ku, Chiba, 263, Japan

[c] Institute for Molecular Science, Myodaiji, Okazaki, 444, Japan

Version of record first published: 24 Sep 2006

PLEASE SCROLL DOWN FOR ARTICLE

Se-SUBSTITUTION AND CATION EFFECTS ON THE HIGH-PRESSURE MOLECULAR SUPERCONDUCTOR, β-Me4N[Pd(dmit)2]2 –A UNIQUE TWO-BAND SYSTEM–

REIZO KATO, YOU-LIANG LIU, YUKO HOSOKOSHI* and SHUJI AONUMA

The Institute for Solid State Physics, The University of Tokyo,
Roppongi 7-22-1, Minato-ku, Tokyo 106, Japan

HIROSHI SAWA

Department of physics, Faculty of Science, Chiba University, Yayoi-cho 1-33, Inage-ku, Chiba 263, Japan

Abstract   Crystal and electronic structures and physical properties of the molecular conductors Me_4Z $[Pd(L)_2]_2$ (Z = N, P, As, and Sb; L = dmit and dmise) are described. Every salt has very similar crystal structure with "solid-crossing" columns. The behavior of resistivity under pressure depends on the Se-substitution and the choice of the cation. Tight-binding band calculations indicate that these salts form a unique two-band system. The narrow and two-dimensional HOMO (anti-bonding) band is thought to form the half-filled conduction band. Magnetic properties suggest that the insulating state under ambient pressure comes from the strong electron-electron correlation. The one-dimensional LUMO (bonding) band is located below the HOMO band. The application of pressure induces an overlap of these two bands and changes the band filling, which brings forth the metallic state. The system under higher pressure, however, shows non-metallic behavior probably due to the one-dimensional instability associated with the LUMO band. Se-substitution and cation effects are observed in the band structure and the shape of Fermi surface. Our results suggest an interrelation between the correlation effect and the dimensionality of the electronic structure.

Keywords: molecular conductor, metal dithiolene complex, resistivity, magnetic susceptibility, crystal structure, metal-insulator transition, pressure effect, band calculation

INTRODUCTION

β-Me4N[Pd(dmit)2]2 (the β-Me4N salt; dmit = 1,3-dithiol-2-thione-4,5-dithiolate) is a

---

* Present address: Institute for Molecular Science, Myodaiji, Okazaki 444, Japan

high-pressure superconductor (T_c=6.2 K at 6.5 kbar).[1] In the low-pressure region (< 4 kbar), this anion radical salt shows no clear metallic behavior. Static magnetic susceptibility is found to be paramagnetic and almost temperature independent apart from a broad maximum at 50-80 K.[1d] ^{1}H-NMR and ESR measurements indicate a magnetic transition at ca. 12 K. All these results suggest that the insulating state in the low-pressure region originates in the strong correlation. An application of pressure induces a metallic behavior and a superconducting transition.[1b]

The electronic state of the molecular conductor strongly depends on physical conditions (pressure, temperature, magnetic field ···etc.) or chemical modifications. The β-Me$_4$N salt can accept a variety of chemical modifications (the central metal, the ligand, and the counter cation). In this paper, we focus our attention on two types of chemical modifications; Se-substitution in the terminal thioxo group of the ligand and replacement of the central atom in the cation (N→P, As, Sb), both of which are examined in combination with the (physical) pressure effect.

In the metal-dmit systems, a large number of peripheral sulfur atoms have a great influence on the intermolecular interaction and the electronic structure. Therefore, the selenium-containing analogs of dmit are of special interest. The selenium atom has more spatially extended orbital and a greater polarizability than the sulfur atom. Cornelissen and co-workers reported α- and β-Me$_4$N[Ni(dmise)$_2$]$_2$ (dmise = 2-selenoxo-1,3-dithiole-4,5-dithiolate) where the terminal thioxo group in the ligand is replaced by the selenoxo group.[2] Such a Se-substitution is expected to enhance the intermolecular interaction with the least difference in the crystal structure. We therefore have selected the Pd(dmise)$_2$ salts to study an effect of enhanced inter-molecular interactions in the metal complex system.
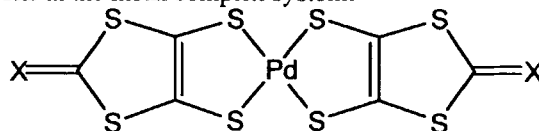
Pd(dmit)$_2$ (X = S)
Pd(dmise)$_2$ (X = Se)

Me$_4$Z[Pd(dmit)$_2$]$_2$ (Z = P, As), both of which have very similar crystal structure to that of the β-Me$_4$N salt, are known to show no high-pressure metallic phase up to 15 and 17.3 kbar, respectively.[3] This indicates that the electronic state of the Pd(dmit)$_2$ system is sensitive to the cation. We have performed a systematic study of the cation effect using Me$_4$Z$^+$ (Z = N, As, P, Sb) cations for the Pd(dmit)$_2$ and Pd(dmise)$_2$ systems.

We concentrate on the resistivity behavior under high pressure. In order to explain the Se-substitution effect and the cation effect, electronic band structures have

been examined with use of the tight-binding approximation.

EXPERIMENTAL

The synthesis of dmise(COPh)$_2$ was carried out according to the literature method except that CH$_3$SO$_3$F was used as a S-methylation reagent.[2] The reaction of the dmise ligand and K$_2$PdCl$_4$ in H$_2$O-methanol followed by an addition of the Me$_4$Z$^+$ cation afforded (Me$_4$Z)$_2$[Pd(dmise)$_2$].

The single crystals of each Me$_4$Z [Pd(dmise)$_2$]$_2$ salt (Z = P, As, Sb) were obtained by the electrochemical oxidation of a solution (20 ml) containing (Me$_4$Z)$_2$ [Pd(dmise)$_2$] (ca. 20 mg) and Me$_4$ZClO$_4$ (30–50 mg) in acetone-acetonitrile (1:1) with a constant current (2.0 μA) at 20°C under an Ar atmosphere. An H-tube (without a frit) and two platinum electrodes (1 mm diameter) were used. For the preparation of single crystals of Me$_4$N[Pd(dmise)$_2$]$_2$, the air oxidation of a solution containing the 2:1 salt (22 mg) and acetic acid (2 ml) in acetone (20 ml) was carried out at room temperature. In every case, single crystals were obtained as black elongated plates.

Single crystals of Me$_4$Sb[Pd(dmit)$_2$]$_2$ were obtained as black plates by the electrochemical oxidation of a solution (20 ml) containing (Me$_4$Sb)$_2$[Pd(dmit)$_2$] (19.3 mg) and Me$_4$SbClO$_4$ (49.4 mg) in acetone-acetonitrile (1:1) with a constant current (4.0 μA) at 20 °C under an Ar atmosphere. An H-tube (without a frit) and two platinum electrodes (1 mm diameter) were used.

The measurements of the static magnetic susceptibility were performed in the 1.8 < T < 300 K temperature range for randomly orientated single crystals using a Quantum Design MPMS SQUID susceptometer.

Electrical resistivity parallel to the **ab** plane was measured by the standard d.c. four-probe method. Gold leads (15 μm diameter) were attached to the sample with carbon paste. Resistivity measurements under high-pressure were performed in a clamp cell with a 1:1 mixture of Fluorinert No. FC70 and No. FC77, as the pressure transmitting medium. The pressure was calibrated with the superconducting transition temperature of Sn.

X-ray diffraction data at room temperature were collected on a MAC Science automated four-circle diffractometer with monochromated Mo Kα radiation (λ= 0.71069 Å; 50 kV, 300 mA) radiation up to 2θ=60° except for Me$_4$As[Pd(dmise)$_2$]$_2$ (2θ = 40°). The intensities were corrected for Lorentz and polarization effects. The analytical absorption correction was carried out. Structures were solved by the direct method and refined with the full-matrix least-squares method. Anisotropic thermal parameters were used for non-hydrogen atoms. All calculations were performed with

220   R. KATO *et al.*

TABLE 1   Crystal Data for $Me_4Z[Pd(dmit)_2]_2$.

Z	P (r.t.)	P (8 K)	Sb
space group	C2/c	C2/c	C2/c
a / Å	14.400(2)	14.218(4)	14.356(7)
b / Å	6.357(1)	6.2880(9)	6.404(1)
c / Å	36.545(6)	36.42(1)	36.893(7)
β / deg.	98.09(1)	97.41(2)	97.54(2)
V / Å^3	3312(1)	3228(1)	3362(1)
total no. of obsd reflctns	5209	—	5289
no. of unique data with $\lvert F_o \rvert > 3\sigma(\lvert F_o \rvert)$	4235	3370	4180
R	0.036	0.037	0.041
R_w	0.042	0.046	0.052

TABLE 2   Crystal Data for $Me_4Z[Pd(dmise)_2]_2$.

Z	N	P	As	Sb
space group	C2/c	C2/c	C2/c	C2/c
a / Å	14.56(1)	14.621(3)	14.614(2)	14.547(5)
b / Å	6.336(4)	6.3396(9)	6.3505(8)	6.389(1)
c / Å	36.48(2)	37.056(6)	37.223(4)	37.470(8)
β / deg.	99.67(5)	99.15(1)	98.87(1)	98.39(2)
V / Å^3	3318(4)	3391.0(9)	3413.3(7)	3445(1)
total no. of obsd reflctns	—	5355	1792	5416
no. of unique data with $\lvert F_o \rvert > 3\sigma(\lvert F_o \rvert)$	—	3562	1325	3149
R	—	0.050	0.038	0.044
R_w	—	0.065	0.040	0.040

TABLE 3   Fractional coordinates and equivalent isotropic thermal
parameters for Me$_4$P[Pd(dmit)$_2$]$_2$ (Room-temperature structure) .

atom	x	y	z	B(eq)
Pd(1)	–0.14914(2)	0.17276(5)	0.518698(8)	1.911(6)
S(1)	–0.08114(7)	0.3371(2)	0.47302(3)	2.48(2)
S(2)	–0.15433(7)	–0.1360(2)	0.48592(3)	2.44(2)
S(3)	–0.13530(7)	0.4764(2)	0.55361(3)	2.32(2)
S(4)	–0.20781(7)	–0.0016(2)	0.56568(3)	2.46(2)
S(5)	–0.03376(8)	0.1798(2)	0.40041(3)	2.77(2)
S(6)	–0.09575(8)	–0.2436(2)	0.41274(3)	2.60(2)
S(7)	–0.17333(8)	0.5595(2)	0.63134(3)	2.92(2)
S(8)	–0.23590(8)	0.1351(2)	0.64165(3)	2.90(2)
S(9)	–0.0288(1)	–0.1465(2)	0.34204(3)	3.92(3)
S(10)	–0.2309(1)	0.4377(3)	0.70378(3)	4.21(3)
P(1)	0	0.2171(3)	1/4	3.12(4)
C(1)	–0.0778(2)	0.1405(6)	0.4419(1)	2.08(7)
C(2)	–0.1083(2)	–0.0643(6)	0.4476(1)	2.00(7)
C(3)	–0.1730(3)	0.3926(6)	0.5934(1)	2.12(7)
C(4)	–0.2030(3)	0.1889(6)	0.5987(1)	2.12(7)
C(5)	–0.0515(3)	–0.0724(7)	0.3833(1)	2.35(8)
C(6)	–0.2143(3)	0.3807(7)	0.6608(1)	2.82(9)
C(7)	–0.0327(4)	0.3767(9)	0.2858(1)	4.4(1)
C(8)	0.0967(4)	0.054(1)	0.2672(2)	4.7(1)
H(1)	0.0189	0.4657	0.2956	4.9
H(2)	–0.0843	0.4650	0.2764	4.9
H(3)	–0.0497	0.2928	0.3052	4.9
H(4)	0.0815	–0.0369	0.2861	5.4
H(5)	0.1140	–0.0336	0.2474	5.4
H(6)	0.1501	0.1361	0.2765	5.4

TABLE 4 Fractional coordinates and equivalent isotropic thermal parameters for Me$_4$P[Pd(dmit)$_2$]$_2$ (at 8K) .

atom	x	y	z	B(eq)
Pd(1)	−0.14885(2)	0.17143(5)	0.518742(6)	0.989(7)
S(1)	−0.07993(7)	0.3367(2)	0.47296(2)	1.16(2)
S(2)	−0.15461(6)	−0.1419(2)	0.48597(2)	1.15(2)
S(3)	−0.13406(6)	0.4799(2)	0.55376(2)	1.12(2)
S(4)	−0.20755(6)	−0.0046(2)	0.56598(2)	1.14(2)
S(5)	−0.03336(7)	0.1769(2)	0.39987(2)	1.16(2)
S(6)	−0.09619(6)	−0.2525(2)	0.41252(2)	1.12(2)
S(7)	−0.17277(6)	0.5658(2)	0.63172(2)	1.14(2)
S(8)	−0.23558(6)	0.1354(2)	0.64227(2)	1.15(2)
S(9)	−0.03047(7)	−0.1554(2)	0.34111(2)	1.30(2)
S(10)	−0.23154(6)	0.4445(2)	0.70439(2)	1.29(2)
P(1)	0	0.2069(3)	1/4	1.16(3)
C(1)	−0.0779(3)	0.1369(7)	0.44166(9)	1.30(8)
C(2)	−0.1082(2)	−0.0667(7)	0.44735(9)	1.33(8)
C(3)	−0.1722(3)	0.3943(7)	0.59389(9)	1.29(8)
C(4)	−0.2026(3)	0.1900(7)	0.59877(9)	1.25(8)
C(5)	−0.0524(2)	−0.0788(7)	0.38240(9)	1.21(8)
C(6)	−0.2139(3)	0.3847(7)	0.66154(9)	1.15(8)
C(8)	0.0994(3)	0.0419(7)	0.2671(1)	1.72(9)
C(9)	−0.0310(3)	0.3706(7)	0.2863(1)	1.50(8)
H(1)	0.0841	−0.0457	0.2865	2.2
H(2)	0.1153	−0.0448	0.2475	2.2
H(3)	0.1519	0.1270	0.2761	2.2
H(4)	0.0203	0.4593	0.2955	2.0
H(5)	−0.0836	0.4566	0.2771	2.0
H(6)	−0.0471	0.2861	0.3059	2.0

TABLE 5   Fractional coordinates and equivalent isotropic thermal parameters for Me$_4$Sb[Pd(dmit)$_2$]$_2$.

atom	x	y	z	B(eq)
Pd(1)	0.14958(2)	0.17812(5)	–0.018654(8)	1.910(6)
S(1)	0.08234(9)	0.3449(2)	0.02661(3)	2.52(2)
S(2)	0.15335(9)	–0.1278(2)	0.01431(3)	2.52(2)
S(3)	0.13526(8)	0.4809(2)	–0.05250(3)	2.40(2)
S(4)	0.20757(8)	0.0072(2)	–0.06602(3)	2.46(2)
S(5)	0.03280(9)	0.1957(2)	0.09838(3)	2.78(2)
S(6)	0.0932(1)	–0.2276(2)	0.08709(3)	2.77(2)
S(7)	0.1704(1)	0.5696(2)	–0.12954(3)	3.10(2)
S(8)	0.2356(1)	0.1523(2)	–0.14104(3)	3.15(3)
S(9)	0.0255(1)	–0.1189(3)	0.15710(4)	4.15(3)
S(10)	0.2263(1)	0.4590(3)	–0.20184(4)	4.68(4)
Sb(1)	0	0.22250(8)	1/4	3.73(1)
C(1)	0.0766(3)	0.1509(7)	0.0572(1)	2.01(7)
C(2)	0.1063(3)	–0.0522(6)	0.0516(1)	1.95(7)
C(3)	0.1722(3)	0.4010(7)	–0.0922(1)	2.24(8)
C(4)	0.2029(3)	0.2001(7)	–0.0981(1)	2.26(8)
C(5)	0.0497(3)	–0.0526(8)	0.1161(1)	2.56(9)
C(6)	0.2112(3)	0.3966(9)	–0.1595(1)	3.0(1)
C(7)	0.0453(5)	0.410(1)	0.2095(2)	5.0(2)
C(8)	–0.1099(5)	0.027(1)	0.2304(2)	5.7(2)
H(1)	0.096	0.498	0.219	5.6
H(2)	0.064	0.328	0.190	5.6
H(3)	–0.006	0.500	0.199	5.6
H(4)	–0.164	0.109	0.220	5.8
H(5)	–0.094	–0.062	0.212	5.8
H(6)	–0.130	–0.056	0.249	5.8

R. KATO *et al.*

TABLE 6 Fractional coordinates and equivalent isotropic thermal parameters for Me$_4$P [Pd(dmise)$_2$]$_2$.

atom	x	y	z	B(eq)
Pd(1)	–0.148394(32)	0.171914(73)	0.519056(12)	1.834(9)
Se(1)	–0.031741(67)	–0.16663(15)	0.342463(22)	4.05(2)
Se(2)	–0.236256(67)	0.45324(18)	0.703306(22)	4.44(2)
S(3)	–0.08096(13)	0.33396(25)	0.474197(45)	2.40(3)
S(4)	–0.15617(13)	–0.13782(25)	0.486745(43)	2.37(3)
S(5)	–0.20699(13)	–0.00039(26)	0.565049(43)	2.46(3)
S(6)	–0.13337(12)	0.47673(25)	0.553393(43)	2.32(3)
S(7)	–0.17246(14)	0.56346(29)	0.629623(46)	2.93(4)
S(8)	–0.23611(13)	0.14092(32)	0.639342(46)	2.93(4)
S(11)	–0.09841(13)	–0.24937(28)	0.415130(44)	2.56(3)
S(12)	–0.03514(13)	0.17136(29)	0.402975(47)	2.75(3)
P(1)	0	0.20206(45)	1/4	3.13(6)
C(1)	–0.07930(40)	0.13572(96)	0.44333(16)	1.8(1)
C(2)	–0.10994(41)	–0.06934(93)	0.44940(15)	1.8(1)
C(3)	–0.17155(45)	0.3950(10)	0.59249(17)	2.2(1)
C(4)	–0.20124(42)	0.1900(10)	0.59731(16)	2.1(1)
C(5)	–0.05512(42)	–0.0805(11)	0.38621(16)	2.2(1)
C(6)	–0.21449(47)	0.3879(12)	0.65782(17)	2.6(1)
C(7)	–0.03048(61)	0.3618(15)	0.28549(24)	4.1(2)
C(8)	0.09656(67)	0.0367(15)	0.26707(27)	4.6(2)
H(1)	0.022	0.452	0.295	4.8
H(2)	–0.081	0.455	0.276	4.8
H(3)	–0.047	0.281	0.305	4.8
H(4)	0.080	–0.053	0.286	5.0
H(5)	0.111	–0.053	0.248	5.0
H(6)	0.149	0.118	0.277	5.0

TABLE 7   Fractional coordinates and equivalent isotropic thermal parameters for Me₄As[Pd(dmise)₂]₂.

atom	x	y	z	B(eq)
Pd(1)	−0.148530(83)	0.17380(20)	0.518979(32)	1.95(3)
Se(1)	−0.03012(14)	−0.15789(34)	0.342883(48)	4.16(5)
Se(2)	−0.23481(14)	0.46370(36)	0.702345(49)	4.60(6)
S(1)	−0.08081(29)	0.33635(67)	0.47434(11)	2.5(1)
S(2)	−0.15570(29)	−0.13526(66)	0.48609(10)	2.5(1)
S(3)	−0.13313(28)	0.47855(65)	0.55345(10)	2.5(1)
S(4)	−0.20761(30)	0.00296(65)	0.56520(11)	2.6(1)
S(5)	−0.03446(30)	0.17444(71)	0.40365(11)	2.8(1)
S(6)	−0.09863(30)	−0.24427(65)	0.41501(11)	2.7(1)
S(7)	−0.17112(30)	0.56841(72)	0.62880(11)	3.0(1)
S(8)	−0.23642(30)	0.15017(75)	0.63879(11)	3.1(1)
As(1)	0	0.20100(43)	1/4	3.51(7)
C(1)	−0.0793(10)	0.1344(24)	0.44391(37)	2.1(4)
C(2)	−0.1136(10)	−0.0631(24)	0.44921(39)	2.2(4)
C(3)	−0.1674(10)	0.3958(24)	0.59228(39)	2.3(4)
C(4)	−0.2028(10)	0.2003(25)	0.59697(37)	2.1(4)
C(5)	−0.0544(10)	−0.0760(24)	0.38646(40)	2.4(4)
C(6)	−0.2116(10)	0.3967(26)	0.65705(40)	2.9(4)
C(7)	0.0338(11)	0.3733(29)	0.21150(44)	4.3(5)
C(8)	−0.1023(13)	0.0275(30)	0.23131(49)	5.3(6)
H(1)	0.085	0.464	0.221	4.8
H(2)	0.051	0.291	0.193	4.8
H(3)	−0.017	0.463	0.201	4.8
H(4)	−0.155	0.112	0.221	5.7
H(5)	−0.087	−0.061	0.212	5.7
H(6)	−0.121	−0.060	0.249	5.7

226   R. KATO *et al.*

TABLE 8   Fractional coordinates and. equivalent isotropic thermal parameters for $Me_4Sb[Pd(dmise)_2]_2$.

atom	x	y	z	B(eq)
Pd(1)	−0.148938(38)	0.177961(87)	0.518926(14)	2.05(1)
Se(1)	−0.026899(72)	−0.13915(17)	0.343439(23)	4.43(2)
Se(2)	−0.232187(76)	0.48023(20)	0.701279(25)	5.19(3)
S(1)	−0.08192(14)	0.34178(30)	0.474423(48)	2.60(4)
S(2)	−0.15515(14)	−0.13005(30)	0.486550(47)	2.60(4)
S(3)	−0.13333(14)	0.48230(30)	0.552280(47)	2.56(4)
S(4)	−0.20767(14)	0.01004(30)	0.565381(49)	2.73(4)
S(5)	−0.03313(14)	0.18585(33)	0.404316(51)	2.97(4)
S(6)	−0.09593(15)	−0.23308(31)	0.415319(53)	2.92(4)
S(7)	−0.16942(16)	0.57539(34)	0.627563(54)	3.32(5)
S(8)	−0.23631(15)	0.16176(38)	0.638672(51)	3.44(5)
Sb(1)	0	0.20493(14)	1/4	4.31(2)
C(1)	−0.07728(47)	0.1452(11)	0.44478(18)	2.3(2)
C(2)	−0.10936(47)	−0.0549(11)	0.44942(18)	2.2(1)
C(3)	−0.16970(50)	0.4037(12)	0.59171(19)	2.5(2)
C(4)	−0.20259(47)	0.2043(12)	0.59623(17)	2.2(1)
C(5)	−0.05047(49)	−0.0620(12)	0.38740(20)	2.6(2)
C(6)	−0.21116(55)	0.4079(14)	0.65561(21)	3.4(2)
C(7)	0.04405(68)	0.3936(16)	0.20923(26)	5.1(3)
C(8)	−0.11135(80)	0.0079(17)	0.22989(27)	6.3(3)
H(1)	0.095	0.481	0.220	6.3
H(2)	0.065	0.309	0.191	6.3
H(3)	−0.005	0.481	0.199	6.3
H(4)	−0.161	0.090	0.220	8.0
H(5)	−0.091	−0.082	0.213	8.0
H(6)	−0.127	−0.072	0.249	8.0

use of a TEXSAN program package of MSC. Although poor quality of crystals prevented the full crystal structure analysis of Me$_4$N[Pd(dmise)$_2$]$_2$, the cell constants and reflection patterns indicate that this salt is isostructural with the other three Pd(dmise)$_2$ salts.

The crystal structure determination at 8 K for Me$_4$P[Pd(dmit)$_2$]$_2$ was performed using the Weissenberg-type imaging plate system (DIP 320S, MAC Science Co., Inc.) equipped with a closed-cycle helium refrigerator (V202 C5LZR, DAIKIN Co.).

RESULTS AND DISCUSSION

Crystal Structure

Crystal data and final fractional coordinates and isotropic thermal parameters are summarized in Tables 1–8. Isostructural Me$_4$Z[Pd(dmit)$_2$]$_2$ (Z=P, As, Sb) and Me$_4$Z[Pd(dmise)$_2$]$_2$ (Z = N, P, As, Sb) salts have very similar crystal structure to that of the β-Me$_4$N salt. The unit cell contains two "solid-crossing" columns along the **a** + **b** and **a** − **b** directions, respectively. These two columns are crystallographically equivalent. Each of them consists of strongly dimerized acceptor molecules with an eclipsed configuration and very short Pd···Pd distance. These columns form conducting layers (Layers 1 and 2) parallel to the **ab** plane which are separated from each other by a cation sheet. Compared with the β-Me$_4$N salt, these salts show some obvious differences in the interrelations between the dimer and the cation (Fig. 1). Therefore we call this structure β'-type.

Although all the salts have very similar molecular arrangement within the conducting layer, there are slight differences in intermolecular spacings and inter-dimer overlapping mode, depending on the ligand and the cation. Spatially extended π orbitals of Se atoms can contribute to an enhancement of the repulsive chalcogen-chalcogen interactions and thus an enlargement of the intra-dimer spacing in the dmise system (Table 9). The intermolecular spacings are also affected by the choice of the cation. The β-Me$_4$N salt shows the largest inter-dimer spacing and the smallest intra-dimer spacing. On the other hand, in the series of β'-type salts, the larger cation tends to enlarge the inter-dimer spacing and reduce the intra-dimer spacing (Table 9). Figure 2 shows the inter-dimer overlapping mode in the β-Me$_4$N salt and in β'-Me$_4$Z[Pd(dmit)$_2$]$_2$ (Z= P, Sb). One can notice that in the β'-salts the larger cation slightly enhances the shift along the short molecular axis direction and this shift in the Me$_4$Sb salt with the largest cation is comparable to that in the β-Me$_4$N salt. Such structural differences affect values of the intermolecular overlap integrals and therefore the electronic structure (*vide infra*).
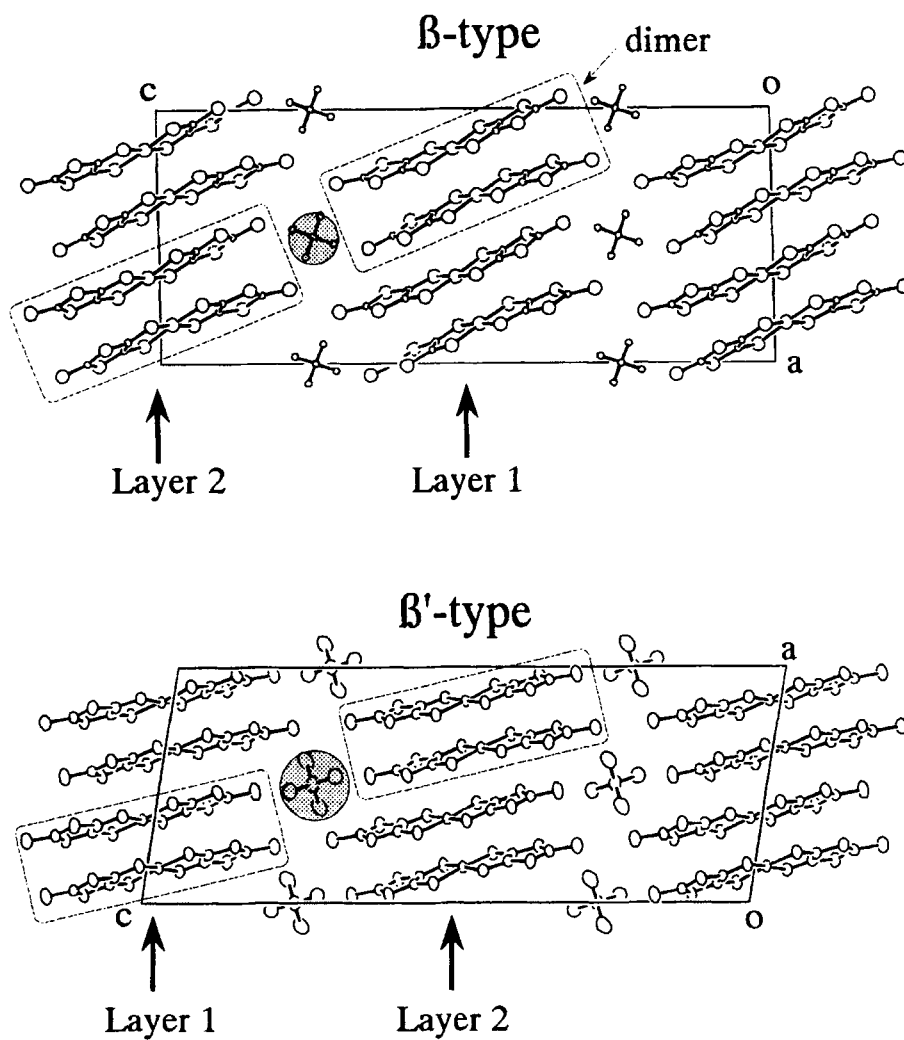
ß-type

β'-type

FIGURE 1   Crystal structures of β- and β'-$Me_4Z[Pd(L)_2]_2$.
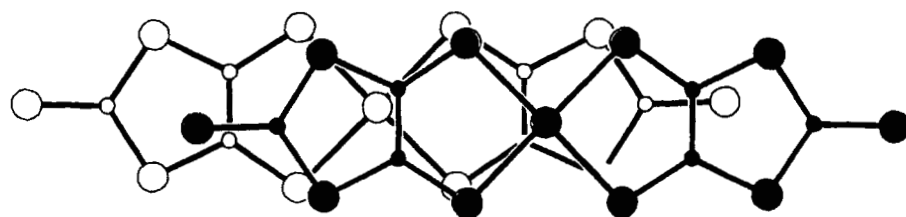
$$Z = N \ (\beta)$$
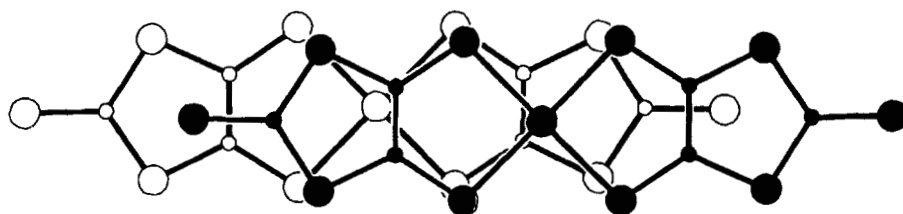
$$Z = P \ (\beta')$$
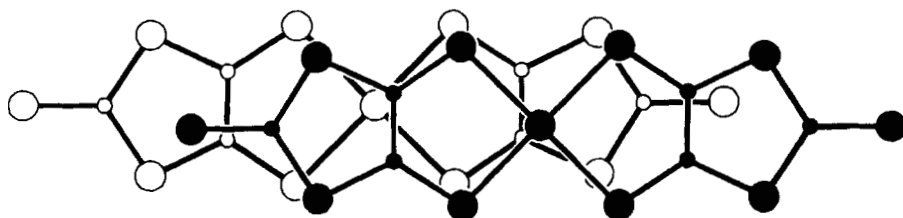
$$Z = Sb \ (\beta')$$

FIGURE 2 Inter-dimer overlapping mode in Me$_4$Z[Pd(dmit)$_2$]$_2$ (Z = N, P, Sb).

TABLE 9 Inter-planar distances (Å) for β- and β'-Me$_4$Z[Pd(L)$_2$]$_2$.

L	type	Z	intra-dimer	inter-dimer	ref.
	β	N	3.28	3.81	1a
dmit	β'	P (r.t.)	3.32	3.72	this work
	β'	P (8 K)	3.32	3.67	this work
	β'	As	3.31	3.71	1a
	β'	Sb-	3.31	3.75	this work
dmise	β'	P	3.36	3.73	this work
	β'	As	3.36	3.75	this work
	β'	Sb	3.34	3.77	this work

In order to understand the nature of the insulating state, we have performed low-temperature X-ray crystal structure analysis on Me$_4$P[Pd(dmit)$_2$]$_2$. At 8 K, very weak reflections that indicate a superlattice (2*a*, 2*b*, *c*) are observed. Such a four-fold structure is also observed in the β-Me$_4$N salt and its origin remains an open question.[1c] The solved crystal structure is an averaged one. Changes in intermolecular spacings (from room temperature to 8 K) are 3.72→3.67 Å (inter-dimer) and 3.32→3.32 Å (intra-dimer), respectively. This result indicates that the inter-dimer interaction associated with the loosely-packed part is more sensitive to the thermal contraction than the intra-dimer interaction. It should be the case in the pressure effect.

Magnetic Susceptibility

Figure 3a shows temperature dependence of the static magnetic susceptibility χ (corrected for diamagnetic contribution) for β'-Me$_4$P[Pd(L)$_2$]$_2$ (L=dmit, dmise). Both salts exhibit a similar paramagnetic behavior with weak temperature dependence and a broad maximum around ca. 120 K. The χ values of Me$_4$P[Pd(dmit)$_2$]$_2$ are comparable to those of the β-Me$_4$N salt and slightly larger than those of Me$_4$P[Pd(dmise)$_2$]$_2$.[1d] Although the temperature dependence of the susceptibility of Me$_4$P[Pd(dmise)$_2$]$_2$ does not clearly manifest a phase transition due to magnetic impurities, the presence of a long-range magnetic ordering below 35 K has been confirmed by recent ^{1}H-NMR study.[4] On the other hand, a small bend can be detected around 42 K in the χ-T curve for Me$_4$P[Pd(dmit)$_2$]$_2$. The magnetization curves measured at 1.8, 2.8, 10, and 30 K show up-turn above ca. 15 kOe, while those measured above 50 K do not show such an up-turn (Fig. 3b). Most plausible origin for this up-turn should be the spin-flop transition. Therefore, the 42 K anomaly in the χ-T curve seems to suggest an existence of some antiferromagnetic transition. As is the case of the β-Me$_4$N salt,[1d] the insulating

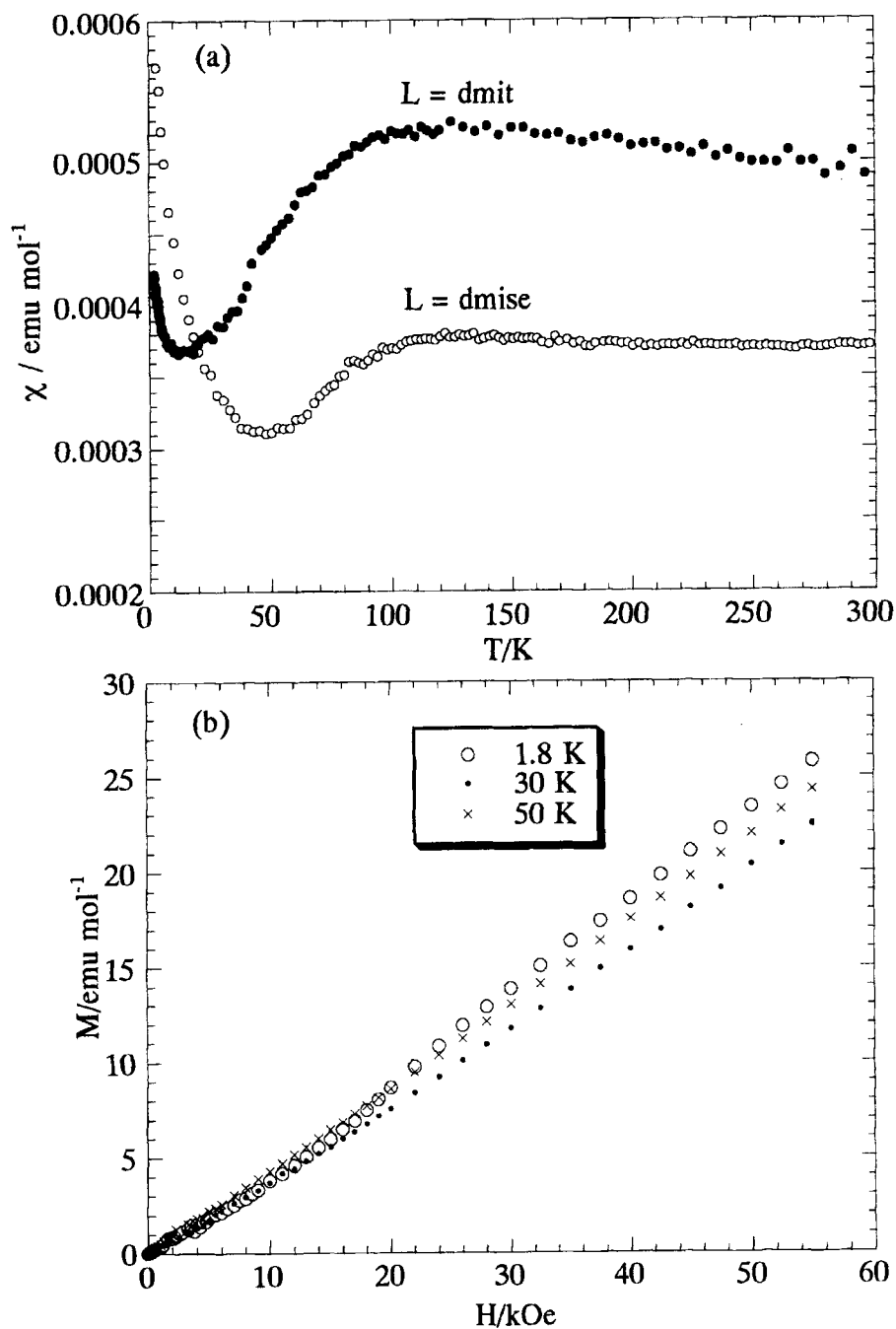FIGURE 3 a) Static magnetic susceptibility for β'-Me₄P[Pd(L)₂]₂ (L = dmit, dmise). Applied fields are 1 kOe for L=dmit and 30 kOe for L=dmise. b) Magnetization curve for β'-Me₄P[Pd(dmit)₂]₂.

state of β'-Me$_4$P[Pd(L)$_2$]$_2$ can be characterized by the paramagnetic behavior accompanied by the long-range magnetic ordering at low temperatures. This might be related to an existence of the strong correlation. However, the nature of the long-range magnetic ordering remains to be explained. More detailed studies on magnetic properties will help to solve the question.

Electrical Resistivity under Pressure

1. dmit system

Under ambient pressure, the temperature dependence of the resistivity for every Me$_4$Z salt is non-metallic. The application of pressure transforms the β-Me$_4$N salt into a superconductor with T$_c$ = 6.2 K (6.5 kbar), while the β'-Me$_4$P and Me$_4$As salts remain non-metallic up to 15 and 17.3 kbar respectively.[3] Figure 4a shows the temperature dependent resistivity of the newly synthesized Me$_4$Sb salt between 1 bar and 13.2 kbar. Under ambient pressure, this salt shows semiconductive behavior with small activation energy values, 0.05 eV (> ca. 250 K), and 0.09 eV (< ca. 250 K). In contrast to the other β'-type salts, the low-temperature insulating behavior of the Me$_4$Sb salt is suppressed by the application of pressure (< ca. 10 kbar). No superconducting transition was observed down to 1.5 K. Under higher pressure, the system shows a rapid increase in the resistivity at the low temperature region as shown in Fig. 4a, indicating a transition to a non-metallic phase. In this pressure region (> ca. 10 kbar), the pressure shifts the transition temperature upwards and makes the transition sharper. In the low-temperature non-metallic phase, the resistivity tends to saturate.

In spite of the similarity in the crystal structure, the pressure dependence of the resistivity is quite sensitive to the choice of the central atom Z. The high-pressure superconductor β-Me$_4$N salt contains the smallest cation. On the other hand, in the β'-type salts, only the Me$_4$Sb salt with the largest cation size shows the metallic behavior under pressure.

2. dmise system

As is the case of the dmit salts, all the dmise salts are non-metallic under ambient pressure. The Me$_4$N salt remains non-metallic up to 15.0 kbar (Fig. 4b). Although the Me$_4$P salt also shows a large increase in the resistibity at low temperatures up to 12.0 kbar, the low-temperature insulating behavior is essentially suppressed above 20.0 kbar (Fig. 4c). It should be noticed that the resistance at 25 kbar is enhanced, compared with that at 20 kbar. In the Me$_4$As salt, the stable metallic phase is observed in the pressure region of 11.5–15.0 kbar. This high-pressure metallic phase, however, becomes unstable at 16.3 kbar (Fig. 4d). Although the low-temperature insulating behavior in the
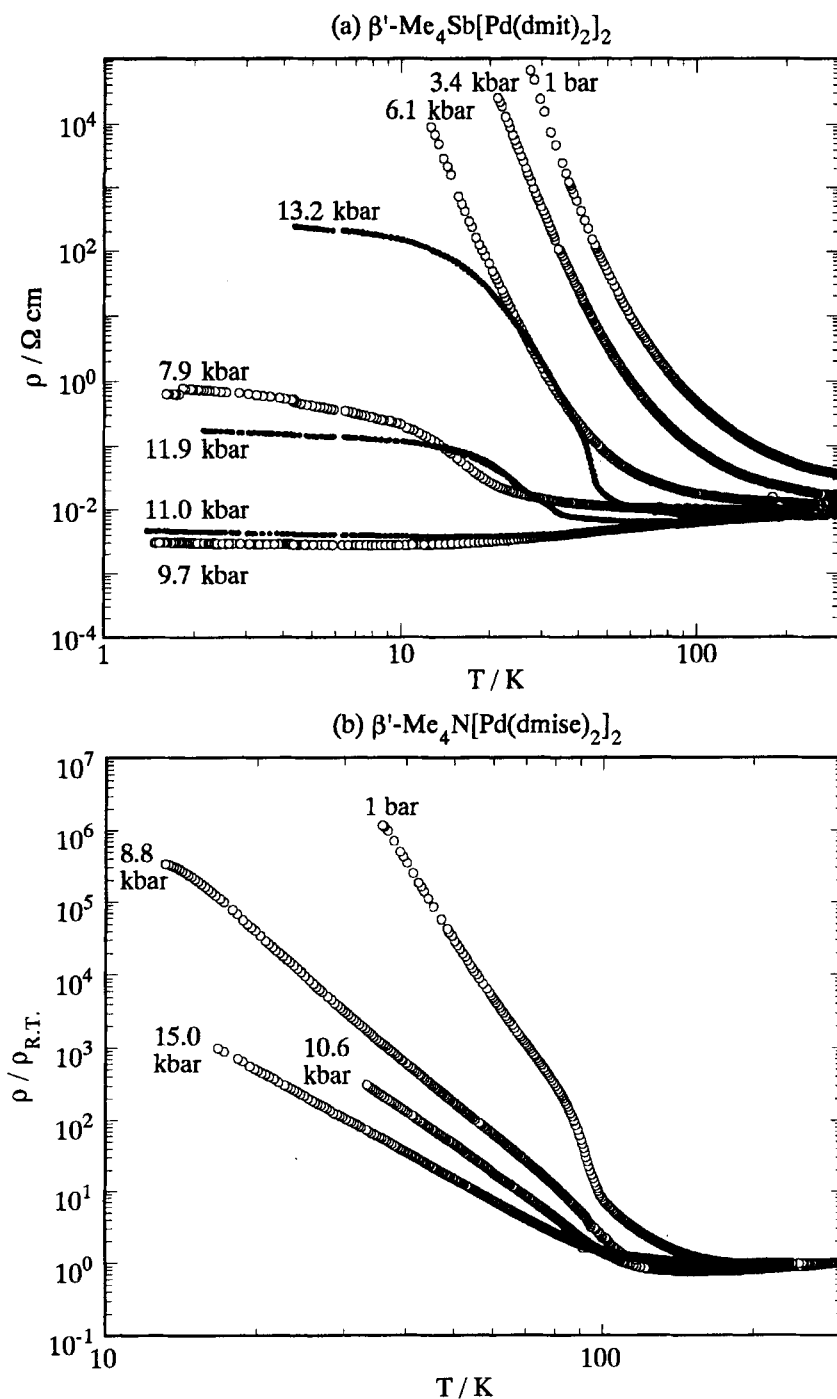
(a) β'-Me$_4$Sb[Pd(dmit)$_2$]$_2$

(b) β'-Me$_4$N[Pd(dmise)$_2$]$_2$

FIGURE 4   Temperature dependence of electrical resistivity at various pressure for β'-Me$_4$Z[Pd(L)$_2$]$_2$ (L = dmit, dmise).

R. KATO *et al.*

(c) β'-Me$_4$P[Pd(dmise)$_2$]$_2$

(d) β'-Me$_4$As[Pd(dmise)$_2$]$_2$

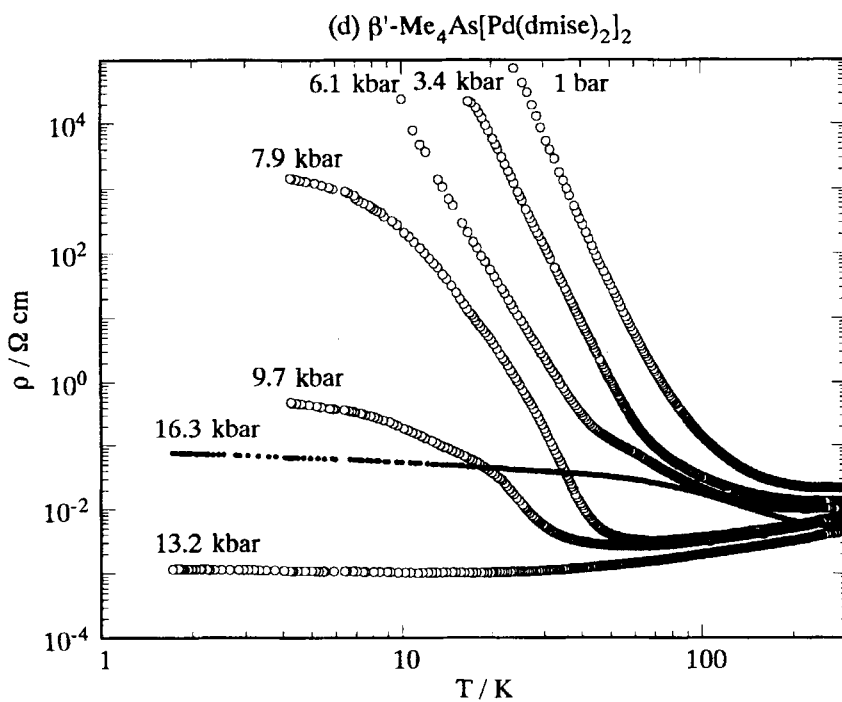FIGURE 4 (continued)
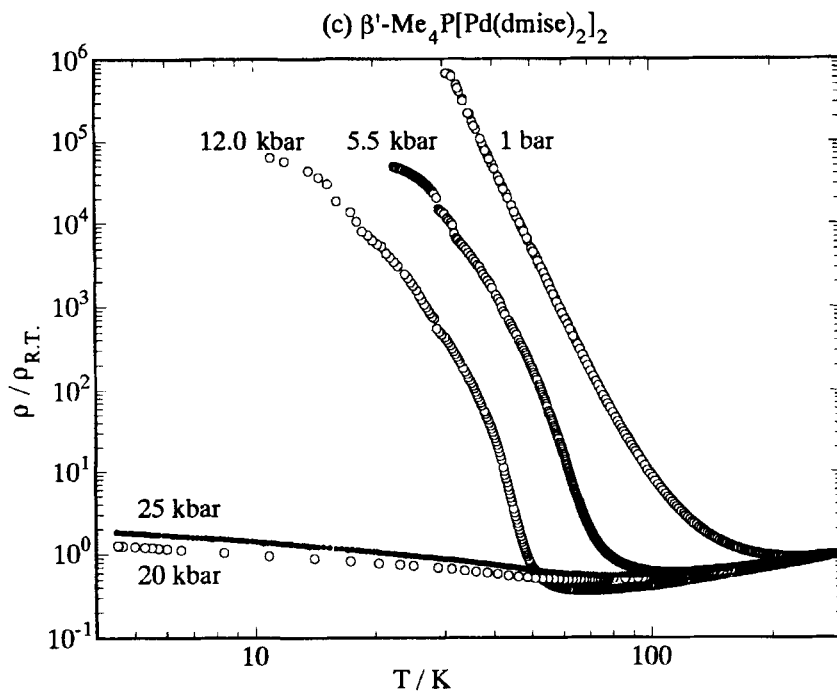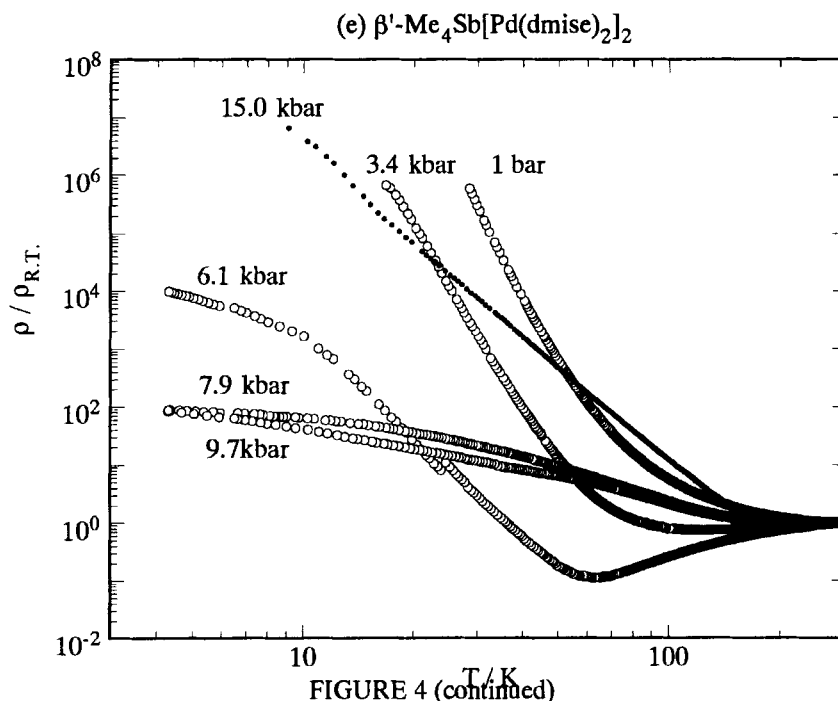
(e) β'-Me$_4$Sb[Pd(dmise)$_2$]$_2$

FIGURE 4 (continued)

Me$_4$Sb salt is barely suppressed in the pressure region of 7.9–9.7 kbar, the low-temperature resistivity rapidly increases above 11.5 kbar (Fig. 4e).

All the dmise salts are the β'-type. The effects of the cation and pressure on this system are very similar to those on the β'-dmit system. The critical pressure, above which the low-temperature insulating phase is suppressed, tends to be lowered by the substitution with the larger cation. And, the non-metallic phase seems to appear again at very high pressure.

Electronic Structure

Recent magnetotransport study has indicated that the tight-binding band calculation can be successfully applied to the metal dithiolene complex system as is the case of other molecular conductors.[5] We therefore consider the Se-substitution and cation effects on the electronic state using this method.

Since the energy gap ΔE between HOMO (highest occupied molecular orbital) and LUMO (lowest unoccupied molecular orbital) is small in the Pd(dmit)$_2$ and Pd(dmise)$_2$ molecules, both of HOMO and LUMO play an important role for the formation of the conduction band.[6] We first calculated inter-molecular overlap integrals among HOMO's and LUMO's which were obtained by the extended Hückel MO calculation with the use of semi-empirical parameters for Slater-type atomic orbitals

TABLE 10 Semiempirical parameters for Slater-type atomic orbitals.

atom	orbital	I_p (Ryd)	ζ_1	ζ_2
C	2s	1.573	1.625	
	2p	0.838	1.625	
S	3s	1.620	2.122	
	3p	0.770	1.827	
Se	4s	1.471	2.122	
	4p	0.809	1.827	
Pd	5s	0.676	2.19	
	5p	0.390	2.15	
	4d	0.949	5.98	2.613
			(0.5264)*	(0.6372)*

* Contraction coefficients used in the double-ζ expansion.

summarized in Table 10.[7] The results are listed in Table 11.

In every salt, the dimeric structure gives rise to alternating large intra-dimer (A) and small inter-dimer (B) overlap integrals along the stacking direction. The b_{1u} symmetry of the HOMO provides larger transverse interactions (p, q, r) than those for the LUMO with b_{2g} symmetry. This means that intermolecular interactions among HOMO's are rather two-dimensional, while those among LUMO's are one-dimensional. It should be mentioned that there are weak inter-molecular interactions between the Layer 1 and the Layer 2 through the terminal S atoms. These values, however, are much smaller than those within the conduction layer and are neglected in the later discussion.

The orbital coefficient of the frontier orbitals for each atom in the $Pd(dmise)_2$ molecule is almost the same with that in the $Pd(dmit)_2$ molecule. The most apparent effect of the spatially extended orbital of the Se atom is an enhancement of the intra-dimer interaction (A) to which the pσ-pσ overlap of the Se orbitals largely contributes.

Comparing the inter-dimer interaction (B), one can see a systematic change in the degree of dimerization according to the variation of the cation. The β-Me_4N salt with the smallest cation exhibits very strong dimerization. In the β'-type salts, the larger cation tends to provide the stronger dimerization, which is consistent with the results of the crystal structure analysis.
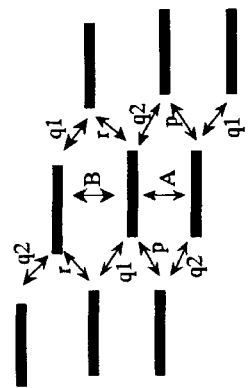
Now we consider the tight-binding band structure.   It has been assumed that the transfer integral (t) is proportional to the overlap integral (S), $t = \varepsilon S$ ($\varepsilon = -10$ eV, ε is a constant with the order of the orbital energies of HOMO and LUMO). According to the

TABLE 11   Intermolecular overlap integrals ($\times 10^3$) among the frontier orbitals (H;HOMO, L;LUMO) in β— and β'–Me$_4$Z[Pd(L)$_2$]$_2$

L = dmit

Z	N			P'			As			Sb		
	L···L	H···H	L···H	L···L	H···H	L···L	L···L	H···H	L···L	L···L	H···H	L···L
A	41.86	-43.92	-0.94	40.97	-44.78	-0.10	41.05	-44.88	-0.85	41.29	-44.84	-1.24
				(40.83)	(-44.57)	(-0.87)						
B	-1.92	-5.35	-0.88	-3.50	-7.11	-1.90	-3.29	-6.78	-1.97	-2.65	-5.91	-1.51
				(-4.57)	(-7.63)	(-2.52)						
p	1.00	-2.37	-0.71	1.24	-3.10	-0.81	1.24	-2.96	-0.88	1.00	-2.36	-0.69
				(1.35)	(-3.79)	(-1.02)						
q1	-0.82	-2.01	-0.41	-0.95	-1.75	-0.38	-0.86	-1.77	-0.31	-0.74	-1.64	-0.28
				(-1.21)	(-2.08)	(-0.43)						
q2	-0.82	-2.01	0.61	-0.95	-1.75	0.58	-0.86	-1.77	0.55	-0.74	-1.64	0.54
				(-1.21)	(-2.08)	(0.66)						
r	1.76	-4.90	-1.44	1.92	-4.34	-1.23	2.03	-4.60	-1.27	2.05	-4.92	-1.34
				(2.42)	(-4.69)	(-1.21)						

* values at 8 K in parentheses

L = dmise

Z	P			As			Sb		
	L···L	H···H	L···H	L···L	H···H	L···L	L···L	H···H	L···L
A	46.07	-58.88	-0.23	46.31	-59.25	-0.74	47.92	-61.07	-0.95
B	-3.30	-7.73	-2.20	-3.42	-8.22	-2.83	-3.26	-6.98	-2.28
p	1.01	-3.24	-0.98	1.00	-3.01	-0.97	0.70	-2.54	-0.93
q1	-0.90	-2.25	-0.68	-1.05	-2.41	-0.56	-0.65	-2.18	-0.63
q2	-0.90	-2.25	0.83	-1.05	-2.41	0.76	-0.65	-2.18	0.77
r	1.06	-4.06	-1.39	1.20	-4.40	-1.56	1.36	-4.93	-1.74

optical data, we adopted the ΔE value of 0.8 eV for both Pd(dmit)$_2$ and Pd(dmise)$_2$ molecules.[6c]   The C-centered cell is reduced to the primitive one as $a_p = (a+b)/2$, $b_p = b$, $c_p = c$. For each of HOMO and LUMO, the dimerization generates the upper (ψ^+ : anti-bonding) and lower (ψ^- : bonding) bands separated by an energy gap. When the inter-stack interactions (p, q, r) could be neglected, this dimerization gap is $2(|t_A| - |t_B|)$ and the band width of each band is $2|t_B|$. (t_A and t_B are transfer integrals corresponding to overlap integrals A and B, respectively). Therefore, in the strongly dimerized system ($|t_A| >> |t_B|$), there exists a large dimerization gap and the effective band width is very narrow. Even if there exist the inter-stack interactions, the situation is similar to the one-dimensional case. Compared with the dimerization gap, the ΔE value in the present system is not so large. Therefore, the ψ^+_{HOMO} band is located higher than the ψ^-_{LUMO} band. Both Pd(dmit)$_2$ and Pd(dmise)$_2$ systems have almost dispersionless LUMO bands with the large dimerization gap. On the other hand, the HOMO bands are dispersive and two-dimensional due to the larger and isotropic inter-dimer interactions. The dimerization gaps in the Pd(dmise)$_2$ system are larger than those in the Pd(dmit)$_2$ system, because the difference between the intra- and inter-dimer interactions (A and B) for each band is larger. Therefore, in the Pd(dmise)$_2$ system, the ψ^-_{LUMO} band is located away from the ψ^+_{HOMO} band, which plays an important role in the consideration of the pressure effect (Fig. 5).

Since the formal charge of the acceptor molecule is $-1/2$, the ψ^+_{HOMO} band is half-filled. When the Coulomb interaction is negligible, the system would behave as the normal metal. On the other hand, when the intra-dimer Coulomb interaction (corresponding to the Hubbard U term) is enough larger than the band width, the ψ^+_{HOMO} band further splits into the lower and upper Hubbard bands. The lower Hubbard band is completely filled, and the system is considered to be a two-dimensional Mott insulator. Magnetic properties suggest that the present system at ambient pressure is close to the Mott insulator

Although there is not enough information about the crystal structure under high-pressure, one can imagine that the dominant pressure effect is to enhance inter-dimer interactions associated with the loosely-packed part.   This means a reduction of the dimerization and leads to an increase in band widths of both HOMO and LUMO bands and to an overlap of these two bands. Therefore, the effective U would be reduced and electron transfer from the ψ^-_{LUMO} band to the ψ^+_{HOMO} band would occur under pressure. And there should be a pressure value above which the ψ^+_{HOMO} band is no longer half-filled. We consider that such a situation is an origin of the high-pressure metallic (and superconducting) behavior in the Pd(dmit)$_2$ and Pd(dmise)$_2$ systems (Fig. 6).   However, we notice that this "band overlap" mechanism is not enough to explain the Se-substitution and cation effects.   For example, this mechanism predicts that it is

β'-Me$_4$P[Pd(dmit)$_2$]$_2$ (r.t.)   β'-Me$_4$P[Pd(dmise)$_2$]$_2$
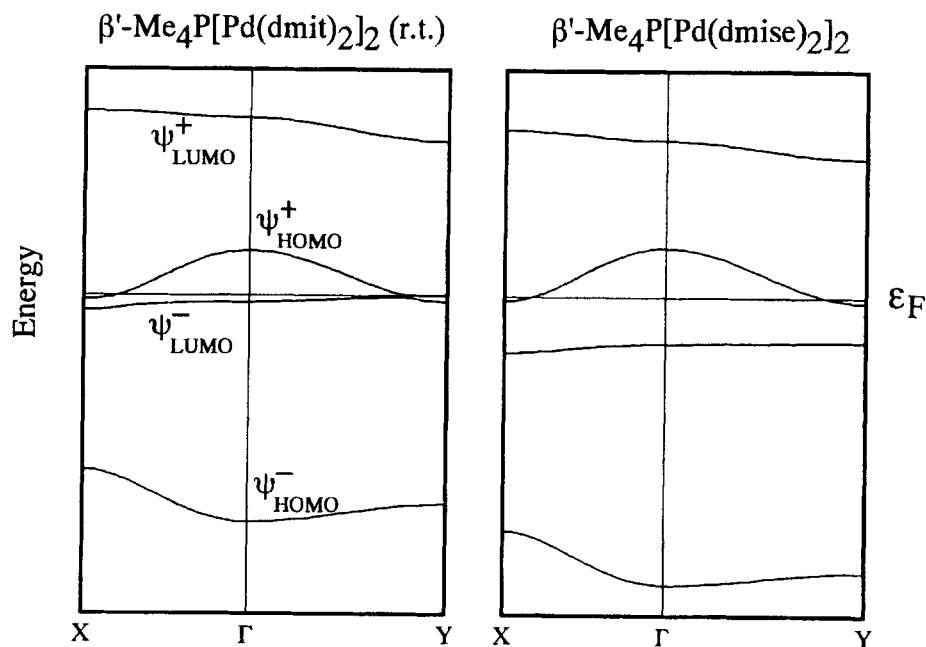
FIGURE 5   Two examples of band structures for β'-Me$_4$Z[Pd(L)$_2$]$_2$.
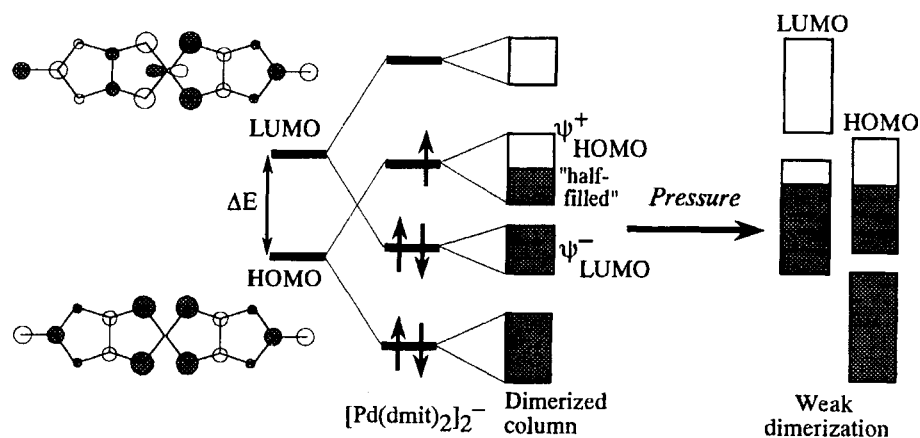
FIGURE 6 Schematic view of the electronic structure for β- and β'-Me$_4$Z[Pd(L)$_2$]$_2$.

easier for the Pd(dmit)$_2$ family with the ψ^-_{LUMO} band located immediately below the ψ^+_{HOMO} band to gain the high-pressure metallic phase. In the Me$_4$As and Me$_4$P salts, however, the high-pressure metallic phase is realized only in the Pd(dmise)$_2$ family. This means that there is another factor which determines the electronic states, in addition to the "band overlap".

We propose the dimensionality of the electronic structure as the second factor. Figures 7 and 8 show calculated Fermi surfaces for β- and β'-Me$_4$Z[Pd(L)$_2$]$_2$ (L= dmit, dmise) at ambient pressure. The shape of the calculated Fermi surface associated with the ψ^+_{HOMO} band varies according to the choice of the cation, which can be related to the degree of the dimerization and the relation with the ψ^-_{LUMO} band. The band calculations and resistivity measurements can be systematically summarized as follows; the high-pressure metallic phase appears more easily in the system with the higher dimensionality. This suggests that the enhanced dimensionality leads to a reduction of the effective Coulomb interaction. Systematic study on the optical properties of the conducting BEDT-TTF (bis(ethylenedithio)tetrathiafulvalene) salts suggests that the correlation effect strongly appears when the system is of one-dimensional character.[8] The similar background would also be relevant for our system.

We consider that the high-pressure non-metallic state can be understood in terms of the one-dimensionality of the LUMO band. In such a high pressure region, the effective U should be reduced. The enhancement of the inter-dimer LUMO$\cdots$LUMO interaction by pressure should be restricted in the stacking direction due to the antisymmetric character of the LUMO.[9] As the LUMO character increases at the Fermi level by high pressure, the one-dimensional character in the Fermi surface develops and leads to the instability of the one-dimensional metal. It is suggestive that in β'-Me$_4$P[Pd(dmit)$_2$]$_2$ the thermal contraction enhances the one-dimensional character as shown in Fig. 7. The saturation of the resistivity in the low-temperature non-metallic phase suggests that two-dimensional part in the Fermi surface still survives down to low temperatures. We imagine that the system turns from a Mott-like insulator in the low-pressure region into a band insulator (and thus a nonmagnetic insulator) in the very high-pressure region.

Our phenomenal understanding can be illustrated in a very schematic view of the low-temperature ground state (Fig. 9). Our results suggest that the electronic state of the present two-band system is determined by two parameters; the "band overlap" and the "dimensionality". The former is coupled with the band width and both of them are closely linked to the degree of the dimerization. The metallic phase spreads over an area away from half-filling and one-dimensionality. At present, we do not have any clear idea concerning a boundary between the Mott-like insulator and the band insulator. Each position for Me$_4$Z[Pd(L)$_2$]$_2$ at ambient pressure is indicated in Fig. 9. Roughly speaking, the Se-substitution affects the band overlap, while the cation affects the dimensionality.
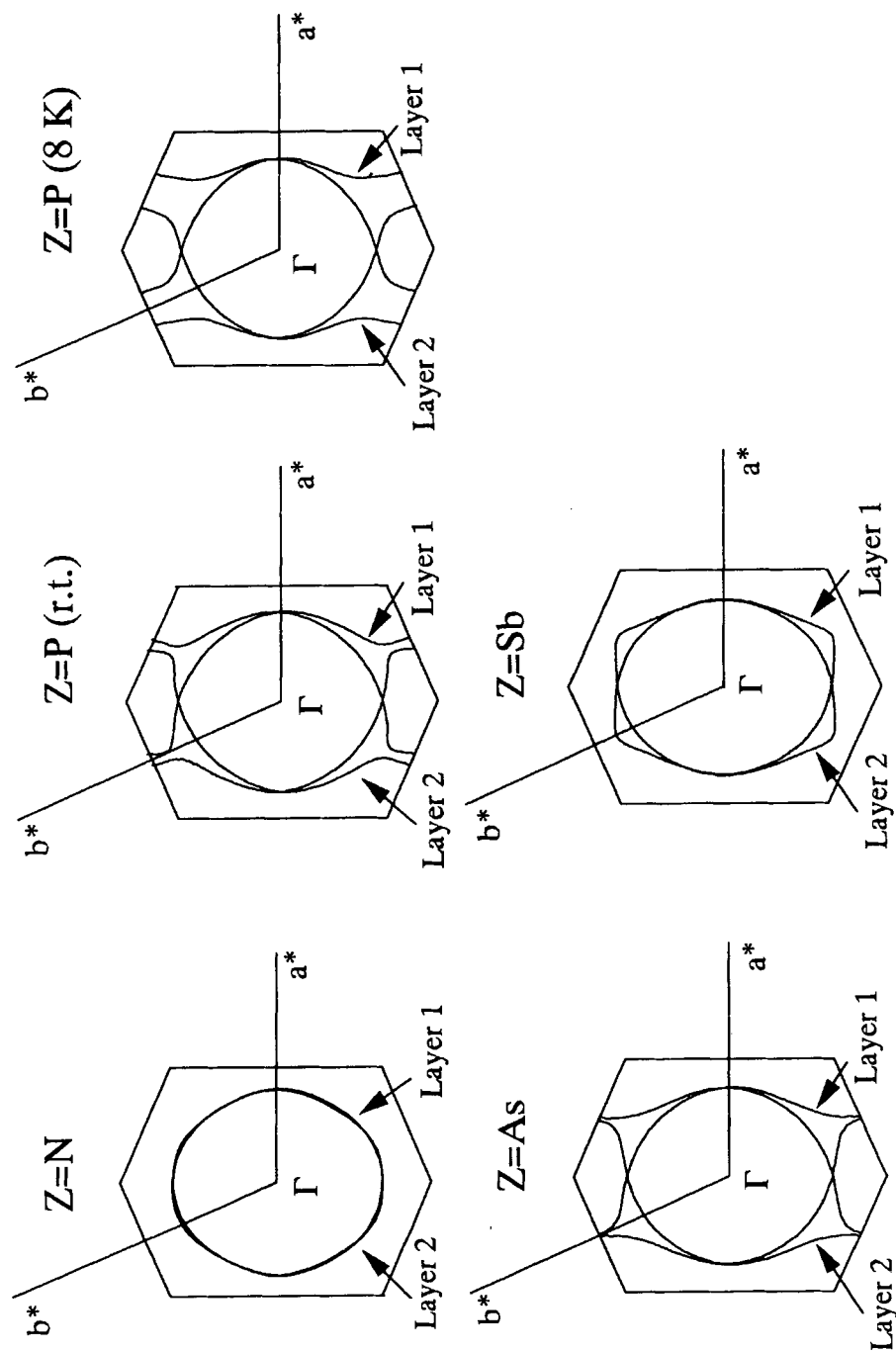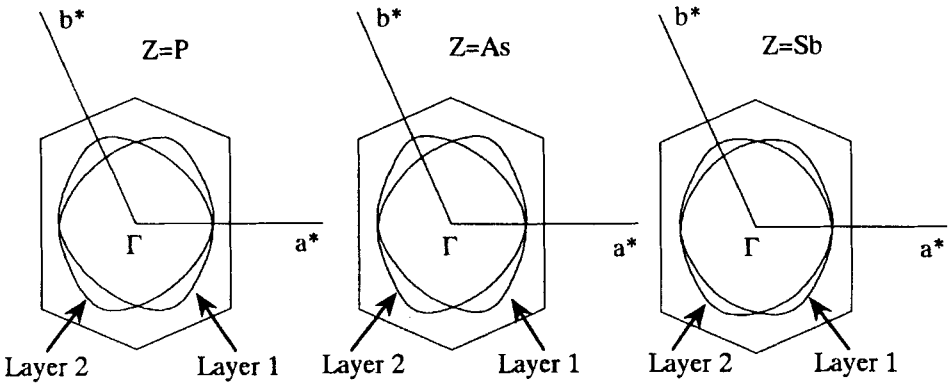
FIGURE 7 Calculated Fermi surfaces for Me$_4$Z[Pd(dmit)$_2$]$_2$.
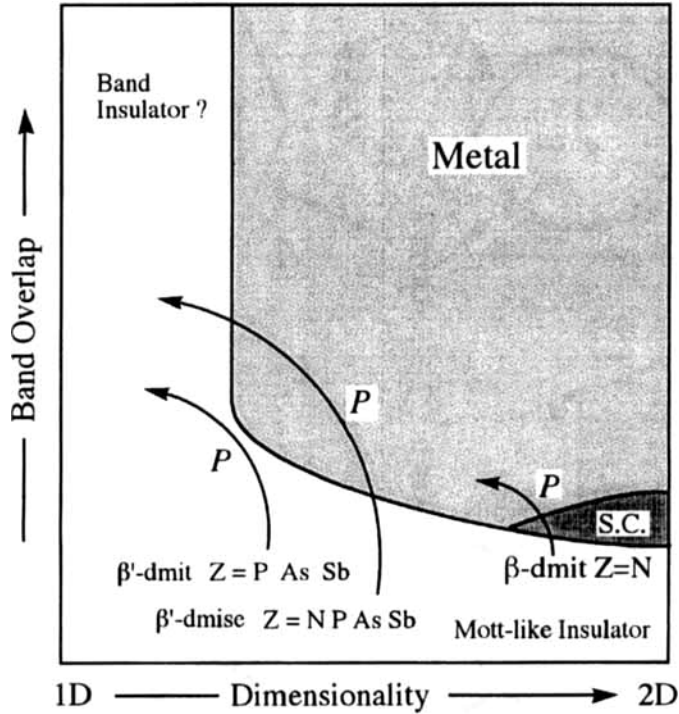
FIGURE 8   Calculated Fermi surfaces for $Me_4Z[Pd(dmise)_2]_2$.

FIGURE 9   Very schematic view of the low-temperature ground state for β- and β'-$Me_4Z[Pd(L)_2]_2$. 'S.C.' is an abbreviation of superconducting phase.

The application of pressure enhances band widths and induces the band overlap. At the same time, the LUMO character at the Fermi level is enhanced, which means the reduction of the dimensionality. Therefore, the system under pressure would change according to arrows labeled by "P " in Fig. 9. Although the β'-dmit family with the smaller dimerization gap is located in the area where the band overlap occurs more easily, the low-dimensional character of the Me$_4$P and Me$_4$As salts tends to carry them to the insulating phase. On the other hand, the β'-dmise family needs higher pressure for the band overlap, but rather strong two-dimensional character brings in the metallic state. The high-pressure superconductor β-Me$_4$N salt has the strong two-dimensional character and is located close to the superconducting phase.

In conclusion, we have proposed a unified view for the unique two-band system β- and β' - Me$_4$Z[Pd(L)$_2$]$_2$ (L= dmit, dmise), where the dimerization is closely linked to the dimensionality of the electronic structure and the band overlap. Our results suggest an interrelation between the correlation effect and the dimensionality.

This paper is dedicated to Professor Yusei MARUYAMA and Professor Fumio OGURA on the occasion of their retirements from Institute for Molecular Science and from Hiroshima University, respectively.

REFERENCES

1. a) A. Kobayashi, H. Kim, Y. Sasaki, K. Murata, R. Kato, and H. Kobayashi, J. Chem. Soc. Faraday Trans., 86, 361 (1990). b) A. Kobayashi, H. Kobayashi, A. Miyamoto, R. Kato, R. A. Clark, and A. E. Underhill, Chem. Lett., 2163 (1991). c) A. Kobayashi, R. Kato, R. A. Clark, A. E. Underhill, A. Miyamoto, K. Bun, T. Naito and H. Kobayashi, Synth. Metals, 56, 2927 (1993). d) K. Seya, Y. Kobayashi, T. Nakamura, T. Takahashi, Y. Osako, H. Kobayashi, R. Kato, A. Kobayashi, and H. Iguchi, Synth. Metals, 70, 1043 (1995).

2. J. P. Cornelissen, B. Pomarède, A. L. Spek, D. Reefman, J. G. Haasnoot, and Reedijk, Inorg. Chem., 32, 3720 (1993).

3. a) C. Faulmann, J-P. Legros, P. Cassoux, J. Cornelissen, L. Brossard, M. Inokuchi, H. Tajima, and M. Tokumoto, J. Chem. Soc. Dalton Trans., 249 (1994). b) T. Naito, Doctor thesis (the University of Tokyo, 1995).

4. Y. Tsuchiya, T. Nakamura, T. Takahashi, Y. -L. Liu, H. Sawa and R. Kato,

Synth. Metals, in press.

5.   a) A. Kobayashi, T. Naito, and H. Kobayashi, Synth. Met., 70,   1047 (1995).
     b) H. Tajima, S. Ikeda, M. Inokuchi, T. Ohta, A. Kobayashi, T. Sasaki, N.
     Toyota, R. Kato, H. Kobayashi, and H. Kuroda, Synth. Met., 70, 1051 (1995).

6.   a) E. Canadell, S. Ravy, J. P. Pouget, and L. Brossard, Solid State Commun., 75,
     633 (1990). b) E. Canadell, I. E. -I. Rachidi, S. Ravy, J. P. Pouget, L. Brossard,
     and J. P. Legros, J. Phys. France, 50, 2967 (1989). c) H. Tajima, T. Naito, M.
     Tamura, A. Kobayashi, H. Kuroda, R. Kato, H. Kobayashi, R. A. Clark, and A.
     E. Underhill, Solid State Commun., 79, 337   (1991).

7.   We carried out the calculation, assuming strictly b_{1u} and b_{2g} symmetries for
     HOMO and LUMO respectively. This assumption compensates experimental errors
     in the X-ray structure analysis.

8.   A. Ugawa, K. Yakushi, and H. Kuroda, Mol. Cryst. Liq. Cryst., 181, 269
     (1990).

9.   A. Kobayashi, H. Kim, Y. Sasaki, R. Kato, and H. Kobayashi, Solid State
     Commun., 62, 57 (1987).